Atmos. Chem. Phys. Discuss., 15, 32519–32560, 2015
www.atmos-chem-phys-discuss.net/15/32519/2015/
doi:10.5194/acpd-15-32519-2015

Atmospheric Chemistry and Physics Discussions

Effects of aerosols on solar radiation in the ALADIN-HIRLAM NWP system

E. Gleeson[1], V. Toll[2,3], K. P. Nielsen[4], L. Rontu[5], and J. Mašek[6]

[1]Met Éireann, Dublin, Ireland
[2]University of Tartu, Tartu, Estonia
[3]Estonian Environment Agency, Tallinn, Estonia
[4]Danish Meteorological Institute, Copenhagen, Denmark
[5]Finnish Meteorological Institute, Helsinki, Finland
[6]Czech Hydrometeorological Institute, Prague, Czech Republic

Received: 2 October 2015 – Accepted: 2 November 2015 – Published: 19 November 2015

Correspondence to: E. Gleeson (emily.gleeson@met.ie)

Published by Copernicus Publications on behalf of the European Geosciences Union.

Abstract

The direct shortwave radiative effect of aerosols in the ALADIN-HIRLAM numerical weather prediction system was investigated using three different shortwave radiation schemes in diagnostic single-column experiments. The aim was to evaluate the strengths and weaknesses of the model in this regard and to prepare the model for eventual use of real-time aerosol information. Experiments were run using ~~observed, climatologically averaged~~ and ~~zero aerosols~~, with particular focus on the August 2010 Russian wildfire case. One of these schemes is a revised version of the HLRADIA scheme with improved treatment of aerosols. Each radiation scheme accurately simulates the direct shortwave effect when observed aerosol optical properties are used rather than climatological-averages or no aerosols which result in large errors, particularly for heavy pollution scenarios. The dependencies of the direct radiative effect of aerosols on relative humidity and the vertical profile of the aerosols on the shortwave heating rates were also investigated and shown to be non-negligible.

1 Introduction

High resolution numerical weather prediction (NWP) models resolve details about local weather. Accurate treatment of the interactions of radiation with clouds and surfaces, and the direct and indirect effects of aerosols, is therefore important. Shortwave (SW) radiation in particular strongly impacts on weather at the surface and the development of the atmospheric boundary layer. Therefore, improvements in the representation of SW radiation are important for ~~the ongoing improvement of~~ NWP forecasts. ~~Accurate~~ SW radiation output from short-range NWP models relies on the accuracy of (1) the assumed amount and distribution of gases, cloud (liquid and ice) and aerosol particles, (2) the parametrization of the cloud, gas and aerosol inherent optical properties (IOPs) and (3) the approximations of radiative transfer through the atmospheric layers. We have previously investigated cloud optical and physical properties, radiative transfer

ACPD
15, 32519–32560, 2015

assumptions and clear-sky gas transmittance in NWP models (Nielsen et al., 2014; Gleeson et al., 2015). This study focusses on the direct radiative influence of aerosols.

Climatological distributions of aerosols are commonly used in present-day operational NWP models when computing the direct radiative effect of aerosols. For example, monthly aerosol climatologies following Tegen et al. (1997) are assumed in ECMWF's (the European Centre for Medium Range Weather Forecasts) global Integrated Forecast System, IFS, and in the ALADIN-HIRLAM limited area modelling system used in this study. However, including a more complete representation of the effects of aerosols in NWP models can make the numerical weather forecast more accurate and is an active area of research (e.g. Mulcahy et al., 2014). Milton et al. (2008) showed that excluding the direct radiative effect of mineral dust and biomass burning aerosols during the dry season in West Africa resulted in an inaccurate representation of the surface energy budget and a warm bias in screen level temperature in forecasts using the UK Met Office Unified Model. Carmona et al. (2008) presented significant correlations between observed aerosol optical depth (AOD) and NWP model temperature errors. Pérez et al. (2006) also demonstrated that including the radiative effects of mineral dust in meteorological simulations can improve the representation of radiative balance, atmospheric temperature and mean sea-level pressure in numerical weather forecasts.

Toll et al. (2015b) showed that the accuracy of ALADIN-HIRLAM forecasts were improved during severe wildfires in summer 2010 in Eastern Europe when the direct radiative effect of the realistic aerosol distribution, as opposed to the Tegen et al. (1997) monthly averages, was included in the model hindcasts. Overall, it is important to include the direct radiative effect of aerosols in order to improve the forecasting of direct and diffuse irradiance for solar energy applications because under clear-sky conditions aerosols mainly affect the SW radiation budget (Breitkreuz et al., 2009).

The IOPs (mass extinction, single scattering albedo (SSA) and asymmetry factor (g) and the direct radiative effect of aerosols depend on the physical properties of the aerosols. Changes in the IOPs of different aerosols types, induced by hygroscopic growth, change the radiative effect of aerosols (e.g. Cheng et al., 2008; Bian

ACPD
15, 32519–32560, 2015

et al., 2009; Markowicz et al., 2003; Zieger et al., 2013). For example, Magi and Hobbs (2003) present measurements of enhanced backscatter by biomass burning aerosols when the relative humidity is high. Pilinis et al. (1995) estimated that the global forcing due to aerosols would double for a relative humidity increase from 40 to 80 %.

The direct radiative effect of aerosols is also dependent on the albedo of the underlying surfaces. Absorbing aerosols may induce a net cooling or a net warming effect depending on the surface albedo and the clouds below the aerosol layer. Chand et al. (2009) estimated that the regional warming induced by absorbing aerosols is three times higher when the covariation for aerosols and cloud cover is included in the calculation. Absorbing aerosols considerably modify the radiative heating rates in the aerosol layer and the vertical profile of temperature. For example Ramanathan et al. (2007) estimated that the 50 year average warming resulting from the so-called atmospheric brown cloud over Asia to be more than 0.5 K over a large area at the 700 hPa level.

Another important aspect to take into account when estimating the direct radiative effect of aerosols is the vertical profile of the aerosols. There are considerable variations in the vertical distributions of aerosols over Europe. Therefore, inaccuracies result from using constant climatological vertical profiles for different aerosol species as is the case in the ALADIN-HIRLAM system. For example, Guibert et al. (2005) analysed the vertical profiles of aerosol extinction over Europe and found that aerosols over southern Europe were concentrated higher in the atmosphere due to the occurence of dust episodes. Meloni et al. (2005) showed that under clear-sky conditions the direct radiative effect of aerosols on radiation at the surface has little dependence on the aerosol vertical profile, but that the vertical profile has an impact on the top of the atmosphere forcing, especially for absorbing aerosols.

The main goal of the present study is to compare the direct SW effect of aerosols in the ALADIN-HIRLAM system using three radiation schemes of varying complexity, with particular focus on an August 2010 Russian wildfire case study. We focus on the direct SW effect of aerosols which is more pronounced than the longwave (LW) effect. MUSC

ACPD
15, 32519–32560, 2015

(Model Unifie Simple Colonne, Malardel et al., 2006), the single column version of three ALADIN-HIRLAM model configurations is used in the sensitivity experiments. Single-column models are extremely useful for developing and testing physical parametrizations and for running idealised experiments that focus on atmospheric physics in a simplified framework. The sensitivity of the direct radiative effect of aerosols to the aerosol vertical profile, relative humidity and the spectral dependence of AOD is studied. Such a study is necessary in order to evaluate the strengths and weakness of the model regarding the treatment of the direct radiative effect of aerosols and for preparation of the model for utilisation of real-time aerosol information. Currently the model relies on the use of external aerosols in the form of monthly climatologies of aerosol optical depth (AOD) at 550 nm and parametrized IOPs (SSA, *g* and AOD scaling) to estimate the direct effect of aerosols on radiation. In the future, the model could obtain aerosol information from chemical transport model simulations, possibly coupled to the NWP model or from the analysis of aerosol observations.

The paper is outlined as follows: the model set-ups are described in Sect. 2; the datasets and experiments carried out are detailed in Sect. 3; the results and discussion are presented in Sect. 4 and conclusions and future work are summarised in Sect. 5.

2 Model set-ups

2.1 ALADIN-HIRLAM ~~configurations and their single column version MUSC~~

The basic configuration of the ALADIN-HIRLAM system used in this study ~~was~~ HARMONIE-AROME based on Seity et al. (2011). ~~In this, the acronym~~ HARMONIE (HIRLAM ALADIN Regional Mesoscale Operational NWP in Europe) ~~is used to denote~~ the specific configuration of the ALADIN-HIRLAM NWP system maintained by the international HIRLAM programme. HARMONIE-AROME uses ALADIN non-hydrostatic dynamics (Bénard et al., 2010), Meso-NH physics (Mascart and Bougeault, 2011) and the SURFEX externalised surface scheme (Masson et al., 2013). Its default set-up for

ACPD
15, 32519–32560, 2015

operational NWP uses a 2.5 km horizontal grid where deep convection is treated explicitly. Surface physiographies are prescribed using the 1 km resolution ECOCLIMAP database and surface elevation is based on GTOPO30 (USGS, 1998). The ALADIN-HIRLAM system can also be used for regional climate simulations (Lindstedt et al., 2015), where the direct radiative effect of aerosols can be of greater importance than in short range NWP applications.

The single column version of the ALADIN-HIRLAM model configurations (MUSC) includes all of the atmospheric and surface parametrizations but ~~excludes~~ large-scale dynamics, horizontal advection, the pressure gradient force and large-scale vertical motion. However, the excluded terms can be estimated by prescribed forcings. Because of the simplifying assumptions, a single-column model is not suitable for real forecasting. Its value lies in the fact that it provides the possibility to study the sensitivity of the model to different formulations of the physical parametrizations for realistic atmospheric conditions.

The time integration in MUSC is done on a single atmospheric column with 65 hybrid model levels. The inputs to MUSC include ~~the initial conditions in the atmosphere, the initial conditions at the surface~~, surface properties and possibly atmospheric forcing data (i.e. temperature, specific humidity and wind speed forcings) applied during the MUSC experiment. These can be derived from the output from a 3-D model experiment. In our experiments the initial state for MUSC was obtained from hourly snapshots of a 3-D HARMONIE-AROME simulation. Single time-step MUSC experiments were then run using each snapshot, which is sufficient for the diagnostics of radiative transfer.

2.2 Aerosols in MUSC

Regarding aerosols, monthly climatologies of vertically integrated AOD at 550 nm (Tegen et al., 1997) for six aerosol (continental, sea, urban, desert, volcanic and background stratospheric) types are available by default in the model. The aerosol IOPs (SSA, g and AOD scaling for each of the six IFS SW radiation bands) are parametrized following Hess et al. (1998) and Koepke et al. (1997). The 550 nm AOD and spectral

ACPD
15, 32519–32560, 2015

IOPs are used directly by the IFS radiation scheme but are spectrally averaged over the six IFS SW intervals before being used by HLRADIA and ACRANEB2. Climatological vertical profiles of the aerosol types are assumed to distribute the aerosols on model levels (Tanre et al., 1984) which results in an exponential decrease in the aerosol attenuation coefficients with height. The spatial distribution of AOD is used to calculate the direct radiative effect of aerosols whereas the indirect radiative effect of aerosols has not yet been extensively studied in the system.

2.3 ~~Tested~~ radiation schemes

In this study we tested three shortwave radiation schemes in the HARMONIE-AROME/MUSC framework (denoted as MUSC hereafter): (1) The IFS radiation scheme based on cycle 25r1 (Morcrette, 1991; White, 2004), which is the default scheme in HARMONIE-AROME, (2) the HIRLAM radiation scheme HLRADIA (Savijärvi 1990; Wyser et al., 1999) including a new treatment of aerosols, (3) the ACRANEB2 scheme (Mašek et al., 2015) from ALARO-1 physics. For the testing, HLRADIA and ACRANEB2 were imported to the HARMONIE-AROME framework.

Each scheme treats the atmosphere as a 1-D column, consisting of a set of plane-parallel homogeneous layers. All grid boxes are split into a cloudy fraction and a clear-sky fraction with no lateral exchanges between them. The three schemes vary in complexity. The IFS scheme is the most complex of the three, consisting of several SW and LW radiation spectral bands. Its complexitity means that it is also computationally slow and is thus called intermittently in an operational forecasting set-up (by default the frequency of radiation computations is every 15 min in HARMONIE-AROME). The HLRADIA scheme is the simplest of the three schemes. As well as being broadband in SW and LW, the radiative transfer equations are parametrized which makes the scheme very fast. The complexity of ACRANEB2 lies between that of IFS and HLRADIA. It is also a broadband scheme but posesses selective intermittency where slowly-varying gaseous transmissions are updated on a time-scale of hours but quickly-varying cloud IOPs, for example, are recomputed at each model time-step.

ACPD
15, 32519–32560, 2015

Atmospheric composition (i.e. aerosols, clouds and atmospheric gases) and the radiative properties of the surface are needed as input for ~~each of~~ the radiation schemes.

3-D cloud liquid and cloud ice particle concentrations and fractional cloud cover used by the radiation schemes are provided by the corresponding parametrization schemes and model dynamics. However, in the sensitivity tests presented in this paper the model was run under clear-sky conditions.

Monthly climatologies of ozone and a fixed composition mixture of CO_2, N_2O, CH_4 and O_2 are used by IFS and ACRANEB2 but the impact of ozone, oxygen and carbon dioxide on SW irradiance in HLRADIA is assumed to be constant over time and space.

Diffuse and direct surface albedos are provided by the SURFEX surface module. Albedos for ~~1~~ ultraviolet, 1 visible and 1 infrared SW band are available from SURFEX and remapped to the 6 bands in IFS. These albedos are spectrally averaged over the six IFS SW intervals for use in ACRANEB2 and HLRADIA. In fact, HLRADIA only uses the broadband diffuse albedo because in this scheme the direct albedo is computed by adding the direct albedo correction factor (i.e. $0.2/(1+\cos(\mathrm{SZA}))-0.12$) to the diffuse albedo (Wyser et al., 1999). In the version of MUSC used in the sensitivity tests, the effects of orography on radiation are not taken into account.

Further details on ~~some of the~~ differences between the three radiation schemes are given in the following sub-sections.

2.3.1 ~~The~~ IFS ~~radiation scheme~~

The default SW radiation scheme in HARMONIE-AROME is the IFS scheme (ECMWF cycle 25R1) with six SW spectral bands (0.185–0.25–0.44–0.69–1.19–2.38–4.00 µm), three in the ultraviolet/visible spectral range and three in the solar infrared range (Mascart and Bougeault, 2011; White, 2004).

There are several SW cloud liquid and cloud ice IOP schemes available in the model. By default, the SW cloud liquid and cloud ice IOPs are calculated with the Fouquart (1987) and the Ebert and Curry (1992) parametrizations respectively. It is also possible to use the Slingo (1989) SW cloud liquid IOP parametrization and the Fu (1996) SW

ACPD
15, 32519–32560, 2015

cloud ice IOP parametrization. The cloud water load is modified by so-called cloud SW and cloud LW inhomogeneity factors before being used for radiation calculations, each of which is set to 0.7 in the default set-up. For detailed tests of the IFS SW cloud physics in the model see Nielsen et al. (2014), who suggested an improved SW cloud IOP scheme, the removal of the cloud inhomogeneity factor, and that the Fu SW cloud ice IOP scheme (Fu, 1996) be used. We followed these suggestions in the tests presented in this paper.

The SW radiative transfer for the clear-sky fraction is calculated using the two-stream equations (Fouquart and Bonnel, 1980) explained by Mascart and Bougeault (2011) where the reflectance and transmittance of the atmospheric layers is calculated similar to Coakley Jr. and Chylek (1975). The scheme uses IOPs (optical depth, SSA, g) of clouds, aerosols and molecules as input where the IOPs of clouds depend on the cloud droplet effective radius ($r_{e,water}$) and cloud ice effective dimension ($d_{e,ice}$). In IFS the Martin et al. (1994) scheme is used to calculate $r_{e,water}$. The Ou and Liou (1995) scheme is the default scheme for cloud ice effective dimension where $r_{e,ice} = 0.5d_{e,ice}$ (i.e. the crystals are assumed to be spherical). However, the advance Sun and Rikus (2000, 2001) scheme is also available; this scheme assumes hexagonal ice cyrstals (i.e. $r_{e,ice} = 0.6435d_{e,ice}$). On the other hand, the two-stream delta-Eddington approximation (Joseph et al., 1976; Fouquart and Bonnel, 1980) is used for the cloudy sky fraction radiative transfer calculations. Thus, the radiative transfer calculations in the clear-sky fractions are different to the radiative transfer calculations in the cloudy sky fractions. The results from tests of both of these radiative transfer approximations are detailed in Sect. 4.3. In the IFS scheme a maxium-random overlap algorithm is employed between cloud layers.

2.3.2 The HLRADIA radiation scheme

One SW spectral band is considered in the HLRADIA scheme and both the clear-sky and cloudy transmittances and absorptances, or radiative transfer, are parametrized in order to make the scheme very fast (Savijärvi, 1990; Wyser et al., 1999). In HLRADIA

ACPD
15, 32519–32560, 2015

$d_{e,ice}$ is parametrized according to Sun and Rikus (2000, 2001). $r_{e,water}$ is based on Martin et al. (1995). The effective radius used in the radiative transfer parametrization is determined from $r_{e,water}$ and r_{eq}, where an ice cloud with particles of size $r_{e,ice}$ has the same IOPs as a water cloud with $r_{e,water} = r_{eq}$. Thus, in the SW in HLRADIA cloud water and ice are treated together. This scheme uses a maximum overlap cloud algorithm.

In older versions of the scheme, aerosols were accounted for using constant coefficients (Savijärvi, 1990). However, the scheme has recently been augmented with parametrizations of the direct and semi-direct effects of aerosols. Direct and semi-direct effects were realised by implementing new fast analytical SW aerosol transmittances, reflectances and absorptances. The 2-stream approximation equations for anisotropic non-conservative scattering described by Thomas and Stamnes (2002) are used for these calculations. HLRADIA uses the GADS/OPAC aerosol IOPs of Koepke et al. (1997) and the IFS aerosols described in the introductory part of Sect. 2 are translated into GADS aerosols following the definition of Morcrette (ECMWF, 2004). The species include soot, minerals (~~nucleus~~, accumulation, coarse and transported modes), sulphuric acid, sea salt (accumulation and coarse modes), water soluble, and water insoluble aerosols. In order to make the calculations fast, the IOPs are averaged over the entire SW spectrum using spectral weightings calculated at a height of 2 km and a solar zenith angle of 45° for a standard mid-latitude summer atmosphere (Anderson et al., 1986) using the libRadtran/DISORT software package (Mayer and Kylling, 2005; Stamnes et al., 1988).

2.3.3 The ACRANEB2 radiation scheme

The ACRANEB2 scheme (Mašek et al., 2015) was developed as part of the ALARO-1 suite of physics parametrizations. Similarly to HLRADIA, it uses a single SW radiation interval (0.245–4.642 µm). ACRANEB2 uses the Reid et al. (1999) conversion formula to diagnose $r_{e,water}$ and the Heymsfield and McFarquhar (1996) equation to parametrize $r_{e,ice}$. Using these, the broadband cloud liquid IOPs were derived from Hu and Stamnes (1993) spectral data and Key et al. (2002) spectral data were used to derive cloud

ACPD
15, 32519–32560, 2015

ice crystal IOPs, where a rough aggregate of hexagonal crystals is used as the most representative of cirrus clouds.

The Ritter and Geleyn (1992) delta two-stream system, including partial cloudiness according to Geleyn and Hollingsworth (1979), is used for both the clear-sky and cloudy radiative transfer calculations in ACRANEB2. The coefficients are computed according to Räisänen (2002), i.e. by averaging the coefficients of all of the radiatively active species, weighted by their optical thicknesses. The scheme uses a delta-linear phase function (similar to the delta-Eddington approximation used in IFS) but with hemispherically constant intensities of diffuse radiation.

Like IFS, ACRANEB2 uses intermittency to reduce computational costs. However, it differs in that the intermittency is partial with slowly evolving gaseous transmissions updated hourly (using a simple correction to the actual sun elevation), but rapidly changing cloud IOPs updated at every model time-step, followed by solving the delta two-stream equations. Such partial intermittency proved to be more accurate than the full intermittency employed by the IFS radiation scheme, which scales broadband SW fluxes using the elevation of the sun but does not recompute the IOPs.

3 Experiments and datasets

Three sets of experiments are ~~detailed in this section~~, (short names for each experiment have been included in brackets): (1) the case study of the summer 2010 Russian wildfires whose smoke plumes affected Estonia (WFEXP), (2) AOD (AODEXP), aerosol vertical profile (VPEXP) and humidity sensitivity tests (RHEXP) and (3) tests of aerosol radiative transfer (RTEXP). A summary of these experiments in terms the aerosols and radiation schemes used is given in Table 1. Further details are provided in subsequent subsections. Tõravere in Estonia on 8 August 2010 was selected to be studied because the smoke had reached the area by then and measurements of aerosol IOPs and broadband radiation fluxes at Tõravere were available from AERONET and BSRN measurements respectively.

ACPD
15, 32519–32560, 2015

3.1 Aerosol data in MUSC

In addition to the aerosol climatology described in Sect. 2, simulations were also run using observed AOD and derived IOPs from the CIMEL sun/sky radiometer measurements recorded at the Aerosol Robotic Network (AERONET, Holben et al., 1998) station in Tõravere, Estonia. The AOD was derived from measurements of the direct SW radiation at various wavelengths (Holben et al., 1998). SSA and g were derived from sky diffuse irradiance measurements using an inversion algorithm by Dubovik and King (2000). Quality controlled (level 2) AERONET data (Smirnov et al., 2000) were used in this study.

3.2 BSRN radiative flux measurements

SW radiation measurements recorded at Tõravere were used in comparisons to simulated fluxes for the August 2010 wildfire case study. These measurements are independent of the AERONET network and are in fact part of the Baseline Surface Radiation Network (BSRN) described by Ohmura et al. (1998). Downwelling SW radiation fluxes ($\mathrm{W\,m^{-2}}$) simulated by a range of different MUSC experiments for Tõravere on 8 August 2010 were compared to measurements recorded at the Tõravere BSRN station (Kallis, 2010).

3.3 Experiments using MUSC

The first suite of aerosol experiments focused on the Russian wildfire case study (WF-EXP) of summer 2010 which affected parts of Eastern Europe including Estonia. Severe thunderstorms coincided with forest fires in the Baltic region on 8 August 2010 (Toll and Männik, 2015). These wildfires (Witte et al., 2011; Huijnen et al., 2012) resulted in one of the worst cases of atmospheric pollution over Estonia in recent decades. The radiative effects of smoke from these wildfires are described by Chubarova et al. (2012).

ACPD
15, 32519–32560, 2015

However, here we have conducted a focused study of the direct radiative effect of the smoke aerosols which reached Tõravere on 8 August 2010.

3-D simulations on a 2.5 km horizontal grid for 8 August 2010, described by Toll et al. (2015a), were carried out to provide meteorological input data for the MUSC experiments for the severe wildfire case study over Tõravere (58.3° N; 26.5° E). Atmospheric and surface fields from the 3-D simulation at hourly intervals were used to generate input data for MUSC sensitivity experiments to ensure realistic time evolution of the forcing. These single column experiments were run assuming clear-sky conditions, obtained by removing cloud water and cloud ice from each of the hourly initial profiles. For the analysis of the results, only output from the first time-step was used each hour.

For the wildfire test case three MUSC experiments were carried out, ~~differing in their treatment of aerosols~~: (1) no aerosols, (2) climatological aerosols and (3) observed aerosols. For tests using observed aerosols, the aerosols were assigned to the land or continental aerosol type with the remaining aerosol categories (there are six categories in the ALADIN-HIRLAM system) set to zero. In this way, the climatological vertical distribution of land aerosols was assumed for the observed IOPs. This assignment affects the SSA, g and wavelength dependence of AOD used by default in the model.

Two variations of the experiment using observed aerosols were carried out. In the first of these, observed AOD at 550 nm and observed aerosol IOPs (SSA, g and wavelength dependence of AOD) were used, whereas in the second, climatological or parametrized aerosol IOPs were used along with observed AOD at 550 nm. Single time-step MUSC experiments were then carried out using hourly forcing from the 3-D experiments for 8 August 2010 for each aerosol experiment separately. As well as this, the experiments were repeated using the three radiation schemes: IFS, HLRADIA and ACRANEB2.

The second suite of experiments consisted of sensitivity tests using MUSC, including tests of AOD at 550 nm (AODEXP), relative humidity (RHEXP) and the vertical distribution of aerosols (VPEXP). The Tõravere location was also used for each of these tests.

ACPD
15, 32519–32560, 2015

In the tests of AOD at 550 nm the AOD was varied from 0 (no aerosols) to 5 (extremely heavily polluted) to investigate its influence on SW radiation fluxes at the surface. Both observed and parametrized aerosol IOPs were tested for each of the three radiation schemes in MUSC.

The effect of relative humidity (varying from 0 to 1) was tested using 550 nm AODs of 0.1 and 1 and parametrized aerosol IOPs. This was only done using the HLRADIA parametrization as the IFS and ACRANEB2 schemes assume a constant relative humidity of 80 %.

To test the effects of the vertical distribution of the aerosols in MUSC the observed 550 nm AOD at 10:00 UTC on 8 August 2010 at Tõravere was arbitrarily chosen. The effect of varying the vertical scale height (h) of land aerosols in the surface-normalized vertical distribution of AOD was investigated. This exponential function distributes the AOD across the 65 model levels in the model.

The final suite of tests presented in this paper focus on aerosol radiative transfer (RTEXP). Accurate aerosol radiative transfer is of equal importance to accurate aerosol IOPs. We therefore tested clear-sky radiative transfer through a homogeneous layer, with optical properties resembling those of aerosols, using the IFS Fouquart and Bonnel (1980) formulation, the IFS delta-Eddington approximation, the HLRADIA formulation and the Ritter and Geleyn (1992) delta-two-stream approximation compared to the accurate DISORT model (Stamnes et al., 1988).

4 Results and discussion

4.1 Russian wildfire case study (WFEXP)

Figure 1b shows the 550 nm AOD from the MACC reanalysis (Inness et al., 2013) over much of Europe on 8 August 2010 compared to the 550 nm climatological AOD in the model (Fig. 1a) which greatly underestimates aerosols when pollution is heavy. The values of the realistic MACC AOD (up to over 3.5) are an order of magnitude higher

ACPD
15, 32519–32560, 2015

than in the default climatology for August. Figure 2 shows the AOD at Tõravere on 8 August 2010 for 7 wavelengths (data from the AERONET archive) which highlights the strong spectral dependence of AOD; AOD is higher for shorter wavelengths. This notable wavelength dependence is characteristic of biomass burning aerosols (Eck et al., 1999). The AOD at 550 nm (Fig. 2), used in some of the model simulations, was calculated using the AERONET AOD at 500 nm and the Ångström exponent in the 440–675 nm spectral interval.

In addition to 550 nm AOD, the model also requires the following inherent IOPs of aerosols in order to calculate the direct radiative effect of aerosols: AOD spectral scaling coefficients and spectral SSA and g. The AOD spectral scaling coefficients are particularly important because of the high dependence of AOD on wavelength for biomass burning aerosols. Observed AOD scaling coefficients for the six SW bands in the model, assumed valid for the land (soot) aerosol, were derived from the spectral AERONET measurements. These coefficients were then used to derive the AOD for the six SW spectral intervals for the IFS radiation scheme.

A broadband AOD scaling coefficient of 0.959, for use in HLRADIA and ACRANEB2, was derived from the six spectral values derived for IFS using spectral weightings from the standard solar spectrum in the lower troposphere described in Sect. 2.2.2. The remaining IOPs, SSA and g for 8 August 2010 at Tõravere are shown in Fig. 3 for four wavelengths. The asymmetry factor varies from 0.56 to 0.7 across the wavelength range with an average value of $g = 0.634$ for broadband applications (HLRADIA and ACRANEB2 schemes). The aerosol scattering, represented by SSA, remains high (close to 0.96) at each wavelength with little SW spectral dependence. A value of 0.955 was used for the broadband cases. This is similar to results by Dubovik et al. (2002) who showed that the typical SSA of smoke from biomass burning in Boreal forests is high. However, the scattering ~~or SSA from the smoke in~~ this Russian wildfire event was in fact higher than ~~for typical aerosols from biomass burning in~~ Boreal forests (Chubarova et al., 2012).

ACPD
15, 32519–32560, 2015

The results of the wildfire test case experiments in terms of downwelling global SW radiation (SWD) at the Earth's surface in comparison to BSRN observations are shown in Fig. 4a and b (continuous lines) for the IFS radiation scheme. The results from HLRADIA and ACRANEB2 are also depicted relative to observations in Fig. 4b (dashed lines and dotted continuous lines). As expected, when the direct radiative effect of aerosols was excluded SWD was overestimated by $\sim 120\,\mathrm{W\,m^{-2}}$ (Fig. 4b, red curves) at midday. When the direct radiative effect of aerosols was accounted for using only the observed AOD at 550 nm, but default (i.e. climatological/parametrized) SSA, g and spectral scaling factors of land aerosols, SWD was underestimated by $\sim 100\,\mathrm{W\,m^{-2}}$ (green curves in Fig. 4b).

This underestimation can be explained by two factors. Firstly, the climatological spectral scaling factors for the IFS land aerosol AOD give a broadband scaling factor that is more than 30 % higher than the factor estimated from the AERONET spectral measurements. Secondly, the differences in the climatological spectral SSA and g values in the model lead to a delta-Eddington optical depth scaling factor ($1 - \mathrm{SSA} \times g^2$, Joseph et al., 1976) that is approximately 15 % lower than observed. The combination of these factors results in a broadband SW AOD of IFS land aerosols that is approximately 15 % larger than the observed value. This can be seen from the cyan curve in Fig. 4b, which shows the results obtained when all of the aerosol IOPs are based on the AERONET observations rather than climatology.

The use of AOD and IOPs derived from AERONET observations gives excellent agreement between the modelled and observed SWD for each of the three radiation schemes. The discrepancy between simulated and observed SWD after 14:00 UTC is due to the development of convective clouds (Toll et al., 2015a) which are not accounted for in the MUSC clear-sky simulations. SWD is underestimated, particularly at high solar angles when the observed 550 nm AOD is used with climatological IOPs.

Overall, the results for the three schemes are similar (mostly to within 10–20 $\mathrm{W\,m^{-2}}$ for global SWD), particularly in their response to the different aerosol cases. The schemes mostly agree to within a few percent at high sun elevations as can be seen in

ACPD
15, 32519–32560, 2015

Fig. 4b ~~for the hours around noon~~. The largest discrepancies occur in the early morning but a detailed investigation into the reasons for this have not been carried out in this study.

Figure 4c shows the unscaled broadband AOD used in HLRADIA and ACRANEB2 for the following three cases: (1) Climatological aerosols (i.e. climatological 550 nm AOD and parametrized/climatological IOPs, black line), (2) Observed 550 nm AOD and IOPs (cyan line) and (3) Observed 550 nm AOD but parametrized IOPs (green line). The broadband AOD shown in this figure can be compared to the observed AOD at Tõravere shown in Fig. 2 for different wavelengths. The broadband AODs were scaled using g and SSA in the HLRADIA and ACRANEB2 SW radiation schemes to produce the broadband SWD fluxes used to generate the HLRADIA and ACRANEB2 curves in Fig. 4b. Therefore, the differences in SWD between the various Tõravere wildfire experiments are mainly due to the differences in the unscaled broadband AOD shown in Fig. 4c.

4.2 Aerosol sensitivity tests

4.2.1 AOD sensitivity (AODEXP)

3-D model input and AERONET observations for 10:00 UTC on 8 August 2010 for Tõravere were used for the AOD sensitivity tests, which show the influence of 550 nm AOD on SWD for each of the radiation schemes for both observed and parametrized IOPs. Global SWD is shown in Fig. 5a and the direct component of this is shown in Fig. 5b. Clearly, in the case of global SWD, the differences between the SW radiation schemes is small compared to the differences between the results when observed rather than parametrized IOPs are prescribed. While this experiment is a sensitivity test, it clearly illustrates the significant effect that the IOPs have on SW radiation. Direct (Fig. 5b) and diffuse fluxes cannot be compared to observations because the direct irradiances assumed in the models include circumsolar irradiances that cover a broader field of view than standard measurements of direct irradiances.

ACPD
15, 32519–32560, 2015

4.2.2 Relative humidity sensitivity (RHEXP)

Tests were done for 550 nm AOD values of 0.1 and 1.0 and parametrized rather than observed aerosol IOPs. 3-D model input files for 10:00 UTC on 8 August 2010 were used as initialisation and the relative humidity was hard-coded to vary between 0.0 and 1.0. In the IFS and ACRANEB2 radiation schemes, the aerosol IOP parametrizations assumes a relative humidity of 0.8 for the climatological land aerosols. In this regard, the HLRADIA scheme is more advanced as its aerosol IOPs vary with relative humidity. This is shown in Fig. 6a where global, direct and diffuse SWD for the HLRADIA scheme is plotted as a function of relative humidity for 550 nm AODs of 0.1 and 1.0. For large AODs (1.0) the influence of relative humidity is significant and of the order of 10 s of $W\,m^{-2}$ for global and direct SWD. Figure 6b shows the relative difference between the HLRADIA and IFS global SWD as a function of relative humidity, where the latter is independent of relative humidity. For AODs close to the climatological value (i.e. 0.1 here) the relative differences between HLRADIA and IFS are very small and negligible at a relative humidity of 0.8. As the humidity deviates from 0.8, particularly for larger AODs, the differences between HLRADIA and IFS grow to ±5 %.

4.2.3 Vertical distribution of aerosols sensitivity (VPEXP)

In these tests of aerosols a 550 nm AOD value of 0.7 for Tõravere on 8 August 2010 (i.e. the observed value at 10:00 UTC) was used. The tests were run using the IFS radiation scheme but the ACRANEB2 scheme uses the same vertical distribution as IFS. However, the vertical profile is not considered in HLRADIA. The surface-normalized vertical distribution of AOD, $\alpha(z)$, has the following exponential form

$$\alpha(z) = \exp(-z/h),$$

where z is the height above the ground and h is a vertical scale height. h has a default value of 1000 m for land aerosols in the model. We varied the scale height h in order to change the distribution of the land aerosols, and to determine its relative effects

ACPD
15, 32519–32560, 2015

on SW radiation and the SW radiative heating rate. For smaller h the aerosols are concentrated closer to the ground while for bigger h they are spread higher into the atmosphere.

The effect of aerosols, and in particular the vertical scale height for land aerosols, on net SW radiation and the SW radiation heating rate as a function of pressure is shown in Fig. 7. The results are scaled relative to the case where aerosols are not included. At each model level, the relative net SW radiation for each of the vertical scale heights, varies by less than 3 % (Fig. 7a). It is reassuring that the variation with scale height is small because the HLRADIA scheme does not consider vertical profile for ~~overall~~ aerosol transmittance. However, in HLRADIA the vertical profile is considered for the heating rates at atmospheric levels. Unlike SW fluxes, where the differences remain~~s~~ within 3 % throughout the atmosphere, the impact on SW heating rates is significant (ratio of up to ~ 1.5 compared to the default vertical profile when the vertical scale height is approximately halved). The main reason for this is presumably that the heating rate is proportional to flux divergence.

4.3 Aerosol radiative transfer (RTEXP)

The IFS radiation scheme uses different two-stream radiative transfer approximations (Joseph et al., 1976; Fouquart and Bonnel, 1980) for aerosols under the clear-sky and cloudy fractions of a given grid box. We tested both of these radiative transfer approximations as well as the two-stream approximation (Thomas and Stamnes, 2002) used in HLRADIA and the Ritter and Geleyn (1992) two-stream approximation in ACRANEB2 and compared the results to the accurate DISORT scheme (Stamnes et al., 1988) run with 30 streams. Sample transmittance results are shown in Figs. 8 and 9 where the optical thickness is varied but the cosine of SZA (μ_0) is set to 0.6, g to 0.7 and SSA to 0.95.

As can be seen from these figures the IFS, HLRADIA and ACRANEB2 radiative transfer approximations give transmittances that are within a few percent of the accurate 30-stream DISORT calculations for optical thicknesses ~~which are~~ less than 1.

ACPD
15, 32519–32560, 2015

Even for optical thicknesses up to 5, the approximations remain within ±12 % of the DISORT results. Thus, it can be concluded that the three (IFS, HLRADIA, ACRANEB2) approximations are sufficiently accurate. Additional results from tests of the IFS delta-Eddington radiative transfer scheme can be found in the ~~supplement to the paper by~~ Nielsen et al. (2014).

5 Conclusions and future work

When the 550 nm AOD and IOPs (spectral AOD scaling, SSA and g) of aerosols are accurately known, the SW direct radiative effect of aerosols is accurately simulated with the IFS, HLRADIA and ACRANEB2 radiation schemes available in the ALADIN-HIRLAM NWP system. Global SWD radiation was underestimated during the wildfire event in summer 2010, especially at high solar angles, when the observed AOD at 550 nm was used with the climatological or parametrized IOPs in each of the radiation schemes rather than the observed IOPs.

This highlights the need for accurate information on both aerosol concentration and aerosol IOPs in order to improve the simulated radiation budget in the model and possibly to result in an improvement in weather forecasts in the future. The model could acquire this information, including the vertical profile of the aerosol properties, from 3-D aerosol IOP estimates from the C-IFS model or chemical transport model simulations coupled to the NWP model.

The IFS, HLRADIA and ACRANEB2 radiative transfer approximations were tested and found to be accurate to within ±12 % even for large aerosol loads.

The dependency of the direct radiative effect of aerosols on the relative humidity and the dependency of the SW heating rates on the vertical distribution of aerosols were shown to be non-negligible. We therefore suggest that a relative humidity dependent parametrization of aerosol IOPs should be used (like in HLRADIA) as well as realistic vertical profiles of aerosols. Nevertheless, as a first approximation, assuming a constant relative humidity and climatological vertical profiles are acceptable.

ACPD
15, 32519–32560, 2015

For cases of heavy pollution the climatological AOD in MUSC is much smaller than observed and when used with either observed or parametrized IOPs, global SWD radiation is overestimated. This is similar to the case where aerosols are completely omitted. This overestimation of global SWD radiation leads to other model errors. Thus, during heavy pollution considerable improvements in the representation of the radiation budget are possible when real rather than climatological aerosols are included.

The influence of improvements in the representation of the direct radiative effect of aerosols on meteorological forecasts needs to be further studied using 3-D simulations. In this study the direct SW radiative effect of aerosols was studied; in the future the indirect effects of aerosols on cloud microphysics and the longwave effect of aerosols also need to be investigated.

Additionally, our results highlight the issues with having IOPs for each aerosol type but a fixed 550 nm AOD. This is important for aerosol data assimilation which should include all of the aerosol IOPs and not only 550 nm AOD.

Acknowledgements. We acknowledge the support of the International HIRLAM-B and ALADIN programmes. This work was also supported by research grant No. 9140 from the Estonian Science Foundation and by institutional research funding IUT20-11 from the Estonian Ministry of Education and Research. We would like to thank Erko Jakobson for his effort in maintaining the Tõravere AERONET site which archives the aerosol data used in this study and Ain Kallis for his effort in maintaining the Tõravere BSRN station whose archived radiation data were used in this study.

References

Anderson, G. P., Clough, S. A., Kneizys, F. X., Chetwynd, J. H. and Shettle, E. P.: AFGL Atmospheric Constituent Profiles (0–120 km), Tech. Rep., AFGL-TR-86-0110, Air Force Geophysics Lab, Hanscom AFB, MA, USA, 1986.

Bénard, P., Vivoda, J., Mašek, J., Smolíková, P., Yessad, K., Smith, C., and Geleyn, J. F.: Dynamical kernel of the Aladin–NH spectral limited-area model: revised formulation and sensitivity experiments, Q. J. Roy. Meteor. Soc., 136, 155–169, 2010.

ACPD
15, 32519–32560, 2015

Bian, H., Chin, M., Rodriguez, J. M., Yu, H., Penner, J. E., and Strahan, S.: Sensitivity of aerosol optical thickness and aerosol direct radiative effect to relative humidity, Atmos. Chem. Phys., 9, 2375–2386, doi:10.5194/acp-9-2375-2009, 2009.

Breitkreuz, H., Schroedter-Homscheidt, M., Holzer-Popp, T., and Dech, S.: Short-range direct and diffuse irradiance forecasts for Sol. Energy applications based on aerosol chemical transport and numerical weather modeling, J. Appl. Meteorol. Clim., 48, 1766–1779, 2009.

Brousseau, P., Berre, L., Bouttier, F., and Desroziers, G.: Background-error covariances for a convective-scale data-assimilation system: AROME–France 3D-Var., Q. J. Roy. Meteor. Soc., 137, 409–422, doi:10.1002/qj.750, 2011.

Carmona, I., Kaufman, Y. J., and Alpert, P.: Using numerical weather prediction errors to estimate aerosol heating, Tellus B, 60, 729–741, 2008.

Chand, D., Wood, R., Anderson, T. L., Satheesh, S. K., and Charlson, R. J.: Satellite-derived direct radiative effect of aerosols dependent on cloud cover, Nat. Geosci., 2, 181–184, 2009.

Cheng, Y. F., Wiedensohler, A., Eichler, H., Heintzenberg, J., Tesche, M., Ansmann, A., and Zhang, Y. H.: Relative humidity dependence of aerosol optical properties and direct radiative forcing in the surface boundary layer at Xinken in Pearl River Delta of China: an observation based numerical study, Atmos. Environ., 42, 6373–6397, 2008.

Chubarova, N., Nezval', Ye., Sviridenkov, I., Smirnov, A., and Slutsker, I.: Smoke aerosol and its radiative effects during extreme fire event over Central Russia in summer 2010, Atmos. Meas. Tech., 5, 557–568, doi:10.5194/amt-5-557-2012, 2012.

Coakley Jr., J. A. and Chylek, P.: The two-stream approximation in radiative transfer: including the angle of the incident radiation, J. Atmos. Sci., 32, 409–418, 1975.

Dubovik, O. and King, M. D.: A flexible inversion algorithm for retrieval of aerosol optical properties from sun and sky radiance measurements, J. Geophys. Res.-Atmos., 105, 20673–20696, 2000.

Ebert, E. E. and Curry, J. A.: A parameterization of ice cloud optical properties for climate models, J. Geophys. Res., 97, 3834–3836, 1992.

Eck, T. F., Holben, B. N., Reid, J. S., Dubovik, O., Smirnov, A., O'neill, N. T., and Kinne, S.: Wavelength dependence of the optical depth of biomass burning, urban, and desert dust aerosols, J. Geophys. Res.-Atmos., 104, 31333–31349, 1999.

ECMWF: 2.5 Input to the radiation scheme, available at: https://software.ecmwf.int/wiki/display/IFS/CY28R1+Official+IFS+Documentation?preview=/36537694/36733237/Physics.pdf (last access: 17 November 2015), 2004.

ACPD
15, 32519–32560, 2015

Fouquart, Y.: Radiative transfer in climate modeling, in: Proceedings of the NATO Advanced Study Institute on Physically-Based Modeling and Simulation of Climate and Climatic Change, Erice, Italy, 11–23 May 1986, edited by: Schlesinger, M. E., Kluwer Academic Publishers, Dordrecht, the Netherlands, 223–283, 1988.

Fouquart, Y. and Bonnell, B.: Computation of solar heating of the Earth's atmosphere: a new parameterization, Contrib. Atmos. Phys., 53, 35–62, 1980.

Fu, Q.: An accurate parameterization of the solar radiative properties of cirrus clouds for climate models, J. Climate, 9, 2058–2082, 1996.

Geleyn J. F. and Hollingsworth, A.: An economical analytical method for the computation of the interaction between scattering and line absorption of radiation, Contrib. Atmos. Phys., 52, 1–16, 1979.

Gleeson, E., Nielsen, K. P., Toll, V., Rontu, L., and Whelan, E.: Shortwave radiation experiments in HARMONIE tests of the cloud inhomogeneity factor and a new cloud liquid optical property scheme compared to observations, ALADIN-HIRLAM Newsletter, 5, 92–106, 2015.

Guibert, S., Matthias, V., Schulz, M., Bösenberg, J., Eixmann, R., Mattis, I., and Vaughan, G.: The vertical distribution of aerosol over Europe – Synthesis of one year of EARLINET aerosol lidar measurements and aerosol transport modeling with LMDzT-INCA, Atmos. Environ., 39, 2933–2943, 2005.

Heymsfield, A. J. and McFarquhar, G. M.: High albedos of cirrus in the tropical pacific warm pool: microphysical interpretations from CEPEX and from Kwajalein, Marshall Islands, J. Atmos. Sci., 53, 2424–2451, doi:10.1175/1520-0469(1996)053<2424:HAOCIT>2.0.CO;2, 1996.

Hess, M., Koepke, P., and Schult, I.: Optical properties of aerosols and clouds: the software package OPAC, B. Am. Meteorol. Soc., 79, 831–844, 1998.

Holben, B. N., Eck, T. F., Slutsker, I., Tanre, D., Buis, J. P., Setzer, A., and Smirnov, A.: AERONET – a federated instrument network and data archive for aerosol characterization, Remote Sens. Environ., 66, 1–16, 1998.

Hu, Y. X. and Stamnes, K.: An accurate parameterization of the radiative properties of water clouds suitable for use in climate models. J. Climate, 6, 728–742, doi:10.1175/1520-0442(1993)006<0728:AAPOTR>2.0.CO;2, 1993.

Huijnen, V., Flemming, J., Kaiser, J. W., Inness, A., Leitão, J., Heil, A., Eskes, H. J., Schultz, M. G., Benedetti, A., Hadji-Lazaro, J., Dufour, G., and Eremenko, M.: Hindcast ex-

ACPD
15, 32519–32560, 2015

periments of tropospheric composition during the summer 2010 fires over western Russia, Atmos. Chem. Phys., 12, 4341–4364, doi:10.5194/acp-12-4341-2012, 2012.
Inness, A., Baier, F., Benedetti, A., Bouarar, I., Chabrillat, S., Clark, H., Clerbaux, C., Coheur, P., Engelen, R. J., Errera, Q., Flemming, J., George, M., Granier, C., Hadji-Lazaro, J., Huijnen, V., Hurtmans, D., Jones, L., Kaiser, J. W., Kapsomenakis, J., Lefever, K., Leitão, J., Razinger, M., Richter, A., Schultz, M. G., Simmons, A. J., Suttie, M., Stein, O., Thépaut, J.-N., Thouret, V., Vrekoussis, M., Zerefos, C., and the MACC team: The MACC reanalysis: an 8 yr data set of atmospheric composition, Atmos. Chem. Phys., 13, 4073–4109, doi:10.5194/acp-13-4073-2013, 2013.
Joseph, J. H., Wiscombe, W. J., and Weinman, J. A.: The Delta–Eddington approximation for radiative flux transfer, J. Atmos. Sci., 33, 2452–2459, 1976.
Kallis, A.: Basic and other measurements of radiation at station Toravere (2010–08), Tartu Observatoorium, Toravere, doi:10.1594/PANGAEA.745066, 2010.
Key, J. R., Yang, P., Baum, B. A., and Nasin, S. L.: Parameterization of shortwave ice cloud optical properties for various particle habits. J. Geophys. Res., 107, AAC7.1–AAC7.10, doi:10.1029/2001JD000742, 2002.
Koepke, P., Hess, M., Schult, I. and Shettle, E. P.: Global Aerosol Data Set, Report No. 243, Max-Planck-Institut für Meteorologie, Hamburg, 1997.
Lindstedt, D., Lind, P., Kjellström, E., and Jones, C.: A new regional climate model operating at the meso-gamma scale: performance over Europe, Tellus A, 67, 24138, doi:10.3402/tellusa.v67.24138, 2015.
Magi, B. I. and Hobbs, P. V.: Effects of humidity on aerosols in southern Africa during the biomass burning season, J. Geophys. Res., 108, 8495, doi:10.1029/2002JD002144, 2003.
Malardel, S., Lac, C., Pinty, J.-P., Thouron, O., Bouteloup, Y., Bouyssel, F., Seity, Y., and Nuissier, O.: Representation of clouds in AROME, in: Proceedings of the ECMWF Workshop on parametrization of clouds in large-scale models, ECMWF, Reading, UK, 2006.
Markowicz, K. M., Flatau, P. J., Quinn, P. K., Carrico, C. M., Flatau, M. K., Vogelmann, A. M., and Rood, M. J.: Influence of relative humidity on aerosol radiative forcing: an ACE-Asia experiment perspective, J. Geophys. Res.-Atmos., 108, 8662, doi:10.1029/2002jd003066, 2003.
Martin, G. M., Johnson, D. W., and Spice, A.: The measurement and parameterization of effective radius of droplets in the warm stratocumulus clouds, J. Atmos. Sci., 51, 1823–1842, 1995.

ACPD
15, 32519–32560, 2015

Mascart, P. J. and Bougeault, P.: The Meso-NH atmospheric simulation system: scientific documentation, Tech. rep., Meteo France, Toulouse, France, 2011.
Masson, V., Le Moigne, P., Martin, E., Faroux, S., Alias, A., Alkama, R., Belamari, S., Barbu, A., Boone, A., Bouyssel, F., Brousseau, P., Brun, E., Calvet, J.-C., Carrer, D., Decharme, B., Delire, C., Donier, S., Essaouini, K., Gibelin, A.-L., Giordani, H., Habets, F., Jidane, M., Kerdraon, G., Kourzeneva, E., Lafaysse, M., Lafont, S., Lebeaupin Brossier, C., Lemonsu, A., Mahfouf, J.-F., Marguinaud, P., Mokhtari, M., Morin, S., Pigeon, G., Salgado, R., Seity, Y., Taillefer, F., Tanguy, G., Tulet, P., Vincendon, B., Vionnet, V., and Voldoire, A.: The SURFEXv7.2 land and ocean surface platform for coupled or offline simulation of earth surface variables and fluxes, Geosci. Model Dev., 6, 929–960, doi:10.5194/gmd-6-929-2013, 2013.
Mašek, J., Geleyn, J. F., Brožková, R., Giot, O., Achom, H. O., and Kuma, P.: Single interval shortwave radiation scheme with parameterized optical saturation and spectral overlaps, Q. J. Roy. Meteor. Soc., doi:10.1002/qj.2653, online first, 2015.
Mayer, B. and Kylling, A.: Technical note: The libRadtran software package for radiative transfer calculations – description and examples of use, Atmos. Chem. Phys., 5, 1855–1877, doi:10.5194/acp-5-1855-2005, 2005.
Meloni, D., Di Sarra, A., Di Iorio, T., and Fiocco, G.: Influence of the vertical profile of Saharan dust on the visible direct radiative forcing, J. Quant. Spectrosc. Ra., 93, 397–413, 2005.
Milton, S. F., Greed, G., Brooks, M. E., Haywood, J., Johnson, B., Allan, R. P., and Grey, W. M. F.: Modeled and observed atmospheric radiation balance during the West African dry season: role of mineral dust, biomass burning aerosol, and surface albedo, J. Geophys. Res.-Atmos., 113, D00C02, doi:10.1029/2007JD009741, 2008.
Morcrette, J. J.: Radiation and cloud radiative properties in the European Centre for Medium Range Weather Forecasts forecasting system, J. Geophys. Res., 96, 9121–9132, doi:10.1029/89JD01597, 1991.
Mulcahy, J. P., Walters, D. N., Bellouin, N., and Milton, S. F.: Impacts of increasing the aerosol complexity in the Met Office global numerical weather prediction model, Atmos. Chem. Phys., 14, 4749–4778, doi:10.5194/acp-14-4749-2014, 2014.
Nielsen, K. P., Gleeson, E., and Rontu, L.: Radiation sensitivity tests of the HARMONIE 37h1 NWP model, Geosci. Model Dev., 7, 1433–1449, doi:10.5194/gmd-7-1433-2014, 2014.
Ohmura, A., Gilgen, H., Hegner, H., Müller, G., Wild, M., Dutton, E. G., and Dehne, K.: Baseline Surface Radiation Network (BSRN/WCRP): new precision radiometry for climate research, B. Am. Meteorol. Soc., 79, 2115–2136, 1998.

ACPD
15, 32519–32560, 2015

Ou, S. C., Liou, K. N., Takano, Y., Rao, N. X., Fu, Q., Heymsfield, A. J., Miloshevich, L. M., Baum, B., and Kinne, S. A.: Remote sounding of cirrus cloud optical depths and ice crystal sizes from AVHRR data: verification using FIRE II IF0 measurements, J. Atmos. Sci., 52, 4143–4158, 1995.

Pérez, C., Nickovic, S., Pejanovic, G., Baldasano, J. M., and Özsoy, E.: Interactive dust-radiation modeling: a step to improve weather forecasts, J. Geophys. Res.-Atmos., 111, D16206, doi:10.1029/2005JD006717, 2006.

Pilinis, C., Pandis, S. N., and Seinfeld, J. H.: Sensitivity of direct climate forcing by atmospheric aerosols to aerosol size and composition, J. Geophys. Res.-Atmos., 100, 18739–18754, 1995.

Ramanathan, V., Ramana, M. V., Roberts, G., Kim, D., Corrigan, C., Chung, C., and Winker, D.: Warming trends in Asia amplified by brown cloud solar absorption, Nature, 448, 575–578, 2007.

Räisänen, P.: Two-stream approximations revisited: a new improvement and tests with GCM data, Q. J. Roy. Meteor. Soc., 128, 2397–2416, doi:10.1256/qj.01.161, 2002.

Reid, J. S., Hobbs, P. V., Rangno, A. L., Hegg, D. A.: Relationships between cloud droplet effective radius, liquid water content, and droplet concentration for warm clouds in brazil embedded in biomass smoke, J. Geophys. Res., 104, 6145–6153, doi:10.1029/1998JD200119, 1999.

Ritter, B. and Geleyn J. F.: A comprehensive radiation scheme for numerical weather prediction models with potential applications in climate simulations, Mon. Weather Rev., 120, 303–325, doi:10.1175/1520-0493(1992)120<0303:ACRSFN>2.0.CO;2, 1992.

Savijärvi, H.: Fast radiation parameterization schemes for mesoscale and short-range forecast models, J. Appl. Meteorol., 29, 437–447, doi:10.1175/1520-0450(1990)029<0437:FRPSFM>2.0.CO;2, 1990.

Seity, Y., Brousseau, P., Malardel, S., Hello, G., Bénard, P., Bouttier, F., and Masson, V.: The AROME-France convective-scale operational model, Mon. Weather Rev., 139, 976–991, 2011.

Slingo, A.: A GCM parameterization for the shortwave radiative properties of water clouds, J. Atmos. Sci., 46, 1419–1427, 1989.

Smirnov, A., Holben, B. N., Eck, T. F., Dubovik, O., and Slutsker, I.: Cloud-screening and quality control algorithms for the AERONET database, Remote Sens. Environ., 73, 337–349, 2000.

ACPD
15, 32519–32560, 2015

Stamnes, K., Tsay, S.-C., Wiscombe, W., and Jayaweera, K.: Numerically stable algorithm for discrete-ordinate-method radiative transfer in multiple scattering and emitting layered media, Appl. Optics, 27, 2502–2509, 1988.

Sun, Z.: Reply to comments by Greg, M. McFarquhar on parameterization of effective cirrus-cloud particles and its verification against observations, Q. J. Roy. Meteor. Soc., 127, 267–271, 2001.

Sun, Z. and Rikus, L.: Parameterization of effective cirrus-cloud particles and its verification against observations, Q. J. Roy. Meteor. Soc., 125, 3037–3055, 2000.

Tegen, I., Hollrig, P., Chin, M., Fung, I., Jacob, D., and Penner, J.: Contribution of different aerosol species to the global aerosol extinction optical thickness: estimates from model results, J. Geophys. Res.-Atmos., 102, 23895–23915, 1997.

Thomas, G. E. and Stamnes, K.: Radiative Transfer in the Atmosphere and Ocean, Cambridge University Press, New York, NY, USA, 2002.

Toll, V. and Männik, A.: The direct radiative effect of wildfire smoke on a severe thunderstorm event in the Baltic Sea region, Atmos. Res., 155, 87–101, 2015.

Toll, V., Männik, A., Luhamaa, A., and Rõõm, R.: Hindcast experiments of the derecho in Estonia on 08 August 2010: modelling derecho with NWP model HARMONIE, Atmos. Res., 158, 179–191, 2015a.

Toll, V., Reis, K., Ots, R., Kaasik, M., Männik, A., Prank, M., and Sofiev, M.: SILAM and MACC reanalysis aerosol data used for simulating the aerosol direct radiative effect with the NWP model HARMONIE for summer 2010 wildfire case in Russia, Atmos. Environ., 121, 75–85, doi:10.1016/j.atmosenv.2015.06.007, 2015.

USGS: GTOPO30, Global 30 Arc Second Elevation Data Set, US Geological Survey, 1998.

White, P. W.: ECMWF: IFS Documentation Cycle CY23r4, Part IV: Physical processes, available at: https://software.ecmwf.int/wiki/display/IFS/CY23R3+Official+IFS+Documentation?preview=/36537681/36733220/Physics.pdf (last access: 17 November 2015), 2004.

Witte, J. C., Douglass, A. R., da Silva, A., Torres, O., Levy, R., and Duncan, B. N.: NASA A-Train and Terra observations of the 2010 Russian wildfires, Atmos. Chem. Phys., 11, 9287–9301, doi:10.5194/acp-11-9287-2011, 2011.

Zieger, P., Fierz-Schmidhauser, R., Weingartner, E., and Baltensperger, U.: Effects of relative humidity on aerosol light scattering: results from different European sites, Atmos. Chem. Phys., 13, 10609–10631, doi:10.5194/acp-13-10609-2013, 2013.

ACPD
15, 32519–32560, 2015

Table 1. Summary of aerosol-radiation experiments, including details of the radiation schemes and aerosol datasets used.

Experiment	SW radiation scheme	Aerosol
WFEXP	IFS, HLRADIA, ACRANEB2	– Observed ~~i.e. observed 550 nm~~ AOD and IOPs (scaling, SSA and *g*) – climatological i.e. climatological 550 nm AOD and IOPs – parametrized i.e. observed 550 nm AOD but climatological IOPs – zero aerosols
AODEXP	IFS, HLRADIA, ACRANEB2	Observed and climatological IOPs
VPEXP	IFS	Observed (but this is arbitrary)
RHEXP	HLRADIA, IFS	Climatological IOPs (but this is arbitrary)
RTEXP	IFS, HLRADIA, ACRANEB2	Wide range of IOPs tested.

ACPD
15, 32519–32560, 2015

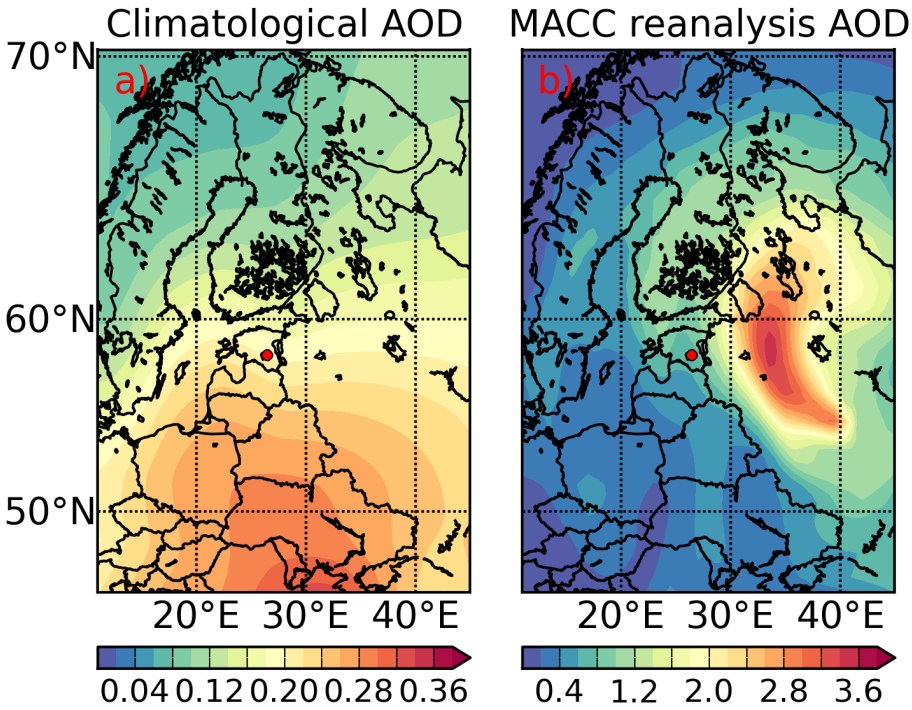

Figure 1. (a) 550 nm AOD for August from the default climatology in ALADIN-HIRLAM (Tegen et al., 1997) **(b)** AOD for 8 August 2010 from MACC reanalysis (Inness et al., 2013). The location of Tõravere (58.3° N; 26.5° E) for which the MUSC experiments are run is shown as a red dot in both panels. Note the factor of 10 difference in AOD between the climatology and the MACC reanalysis.

ACPD
15, 32519–32560, 2015

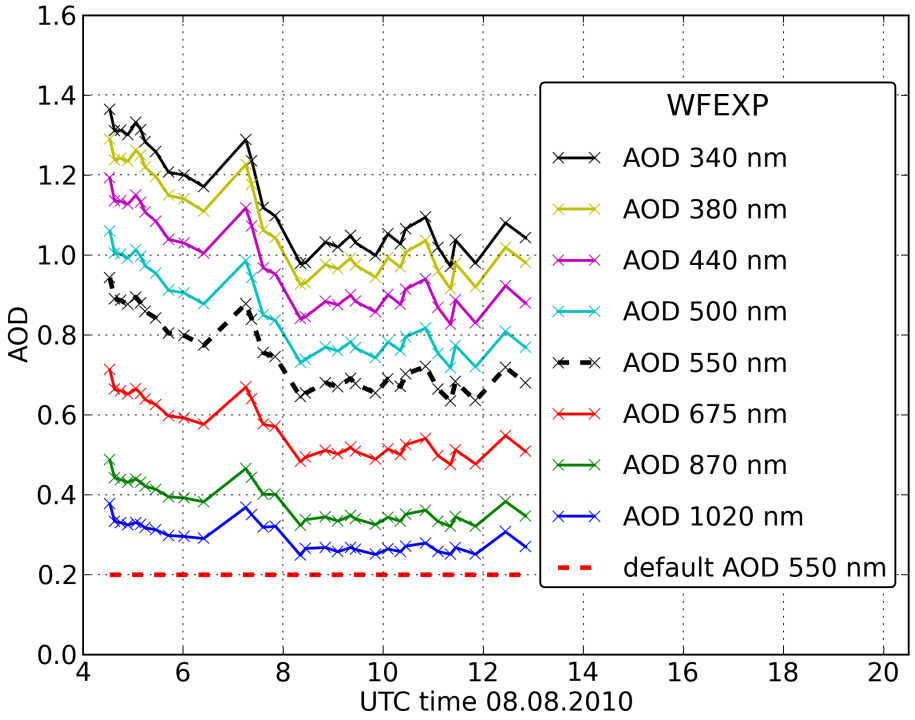

Figure 2. AERONET measurements of AOD at Tõravere on 8 August 2010 for 7 SW wavelengths (nm). The derived 550 nm AOD for Tõravere in August (black dashed line) and the default constant climatological 550 nm AOD (red dashed line) are also shown in the figure. Data are not available after 14:00 UTC due to the presence of clouds.

ACPD
15, 32519–32560, 2015

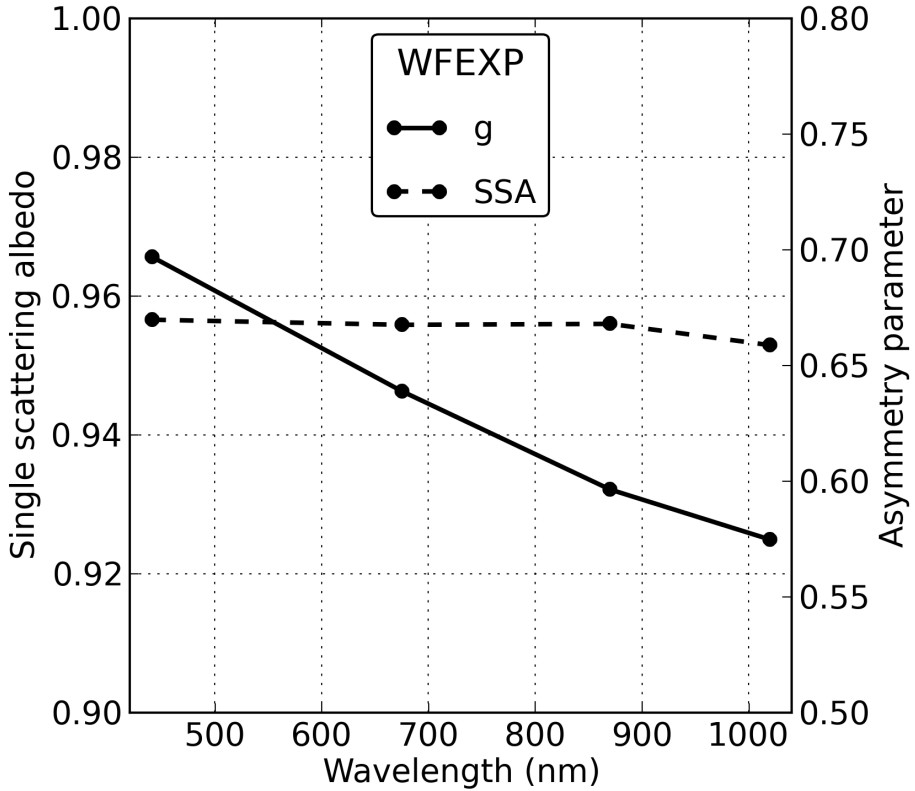

Figure 3. Single scattering albedo (SSA) and asymmetry factor (g) at Tõravere on 8 August 2010 as a function of wavelength attained from the AERONET inversion products database. The data are averaged over the day – data at three different times were available but the time dependence was small.

ACPD
15, 32519–32560, 2015

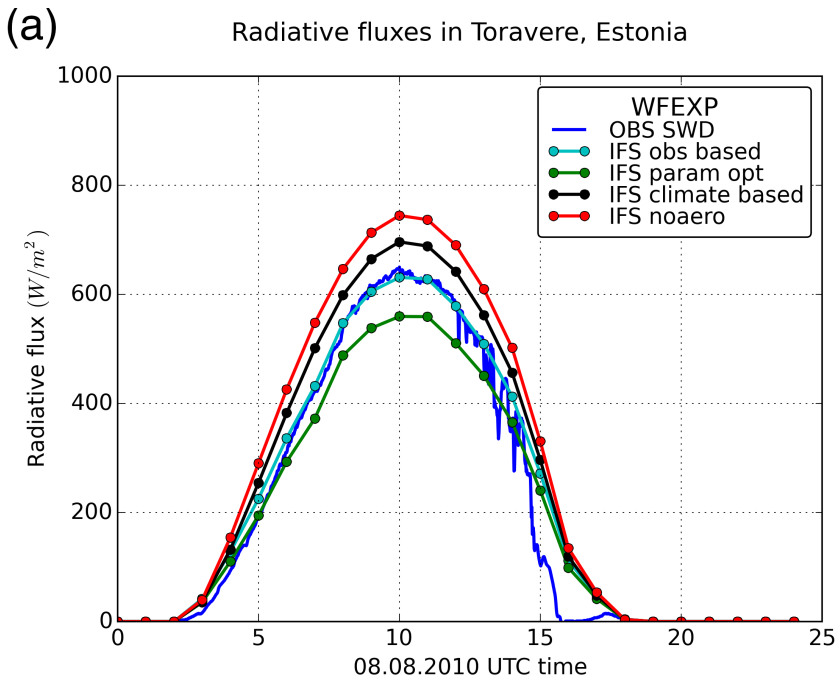

Figure 4.

ACPD
15, 32519–32560, 2015

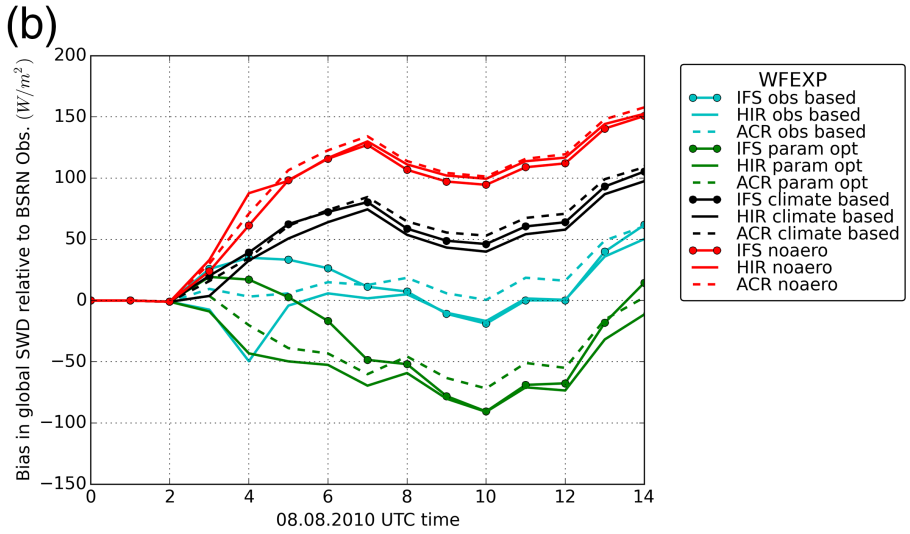

Figure 4.

ACPD
15, 32519–32560, 2015

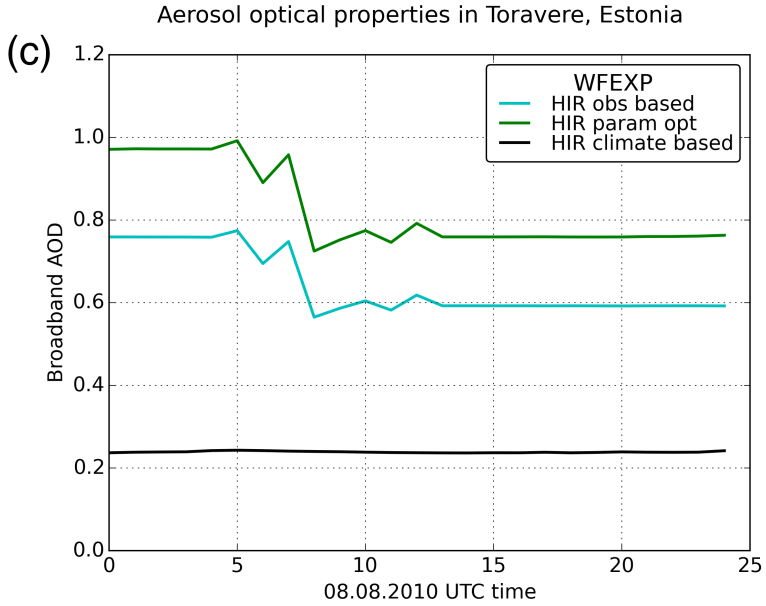

Figure 4. Simulated global SWD radiation flux ($W m^{-2}$) for Tõravere on 8 August 2010, compared to measurements recorded at the Tõravere BSRN station (Kallis, 2010) for a range of aerosol options using **(a)** the IFS scheme **(b)** IFS, HLRADIA and ACRANEB2 biases relative to observations. The broadband AOD used in the HLRADIA and ACRANEB2 experiments is shown in subplot **(c)**. In Fig. 4b only data up to 14:00 UTC are shown because clouds develop after that and are not included in the MUSC simulations. (obs based = observed 550 nm AOD and IOPs (scaling, SSA and *g*); param opt = observed 550 nm AOD but parametrized or climatological IOPs; climate based = climatological 550 nm AOD and IOPs; no aero = zero aerosols).

ACPD
15, 32519–32560, 2015

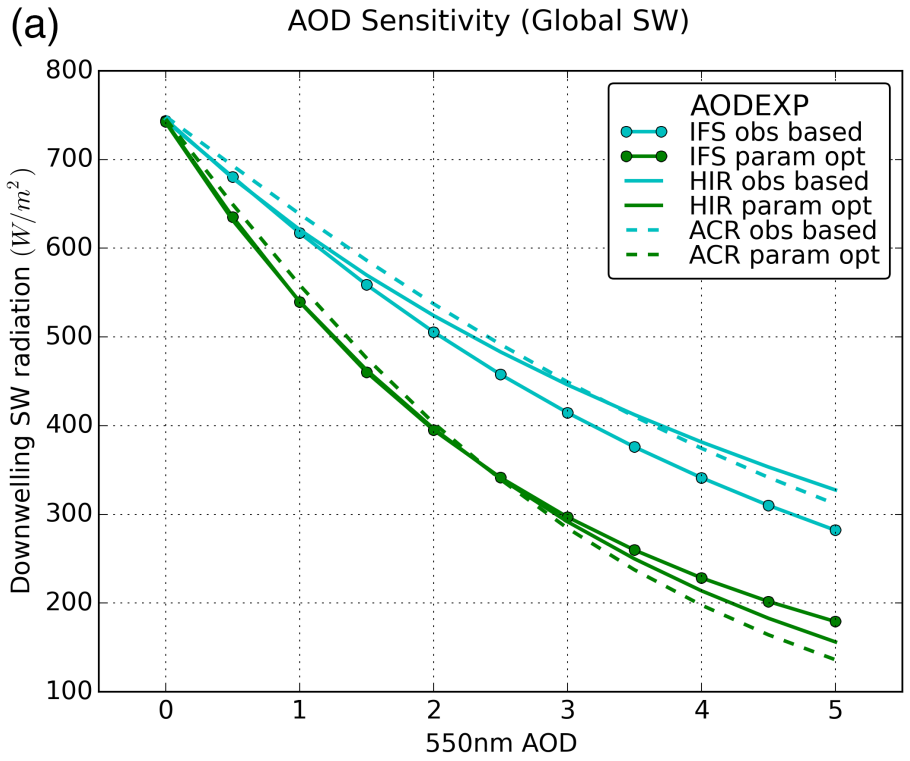

Figure 5.

ACPD
15, 32519–32560, 2015

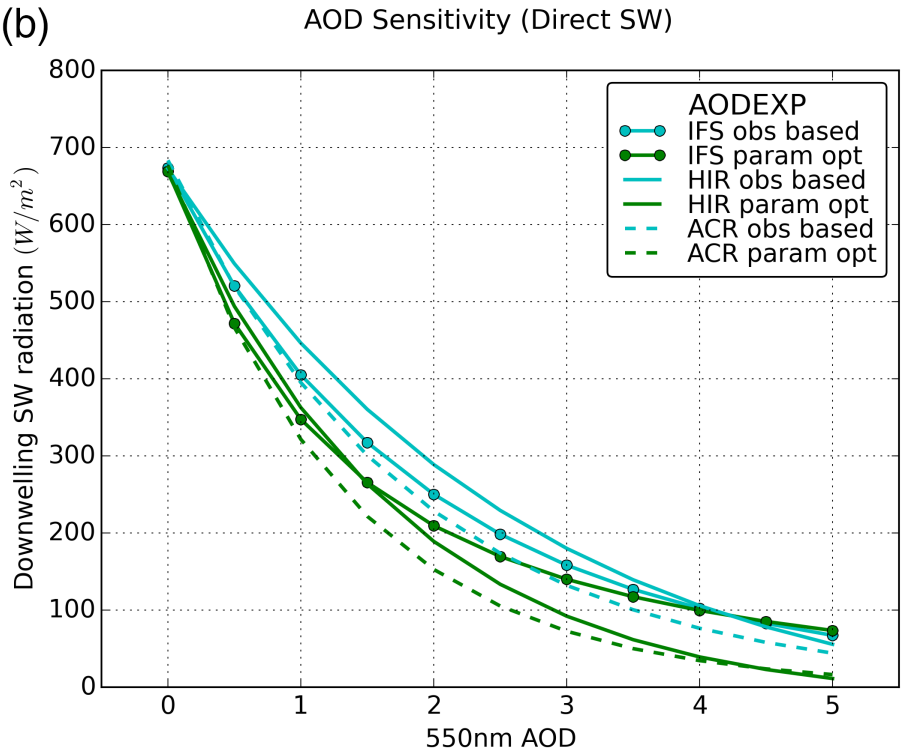

Figure 5. (a) Global SWD as a function of 550 nm AOD for the IFS, HLRADIA and ACRANEB2 radiation schemes and observed or parametrized aerosol IOPs **(b)** similar to **(a)** but direct SWD is shown.

ACPD
15, 32519–32560, 2015

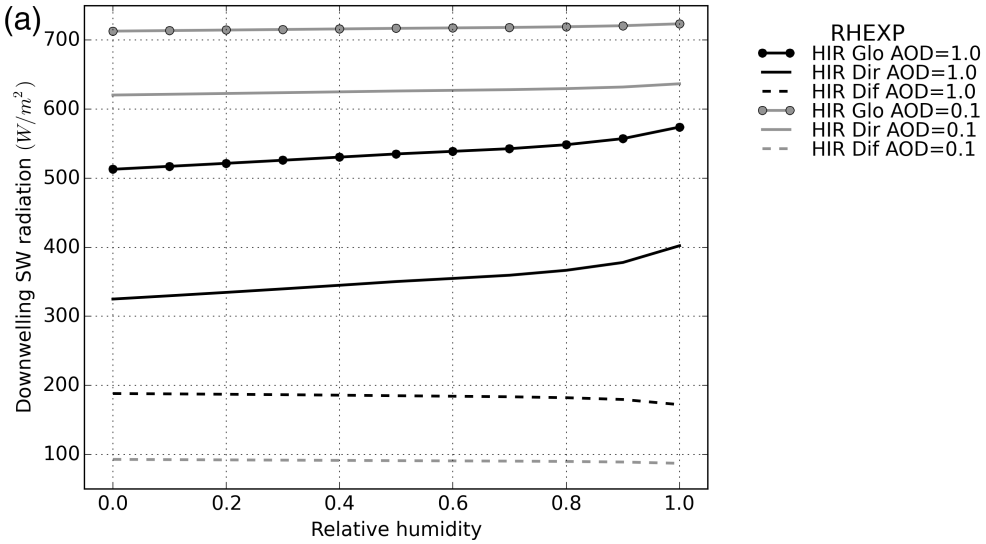

Figure 6.

ACPD
15, 32519–32560, 2015

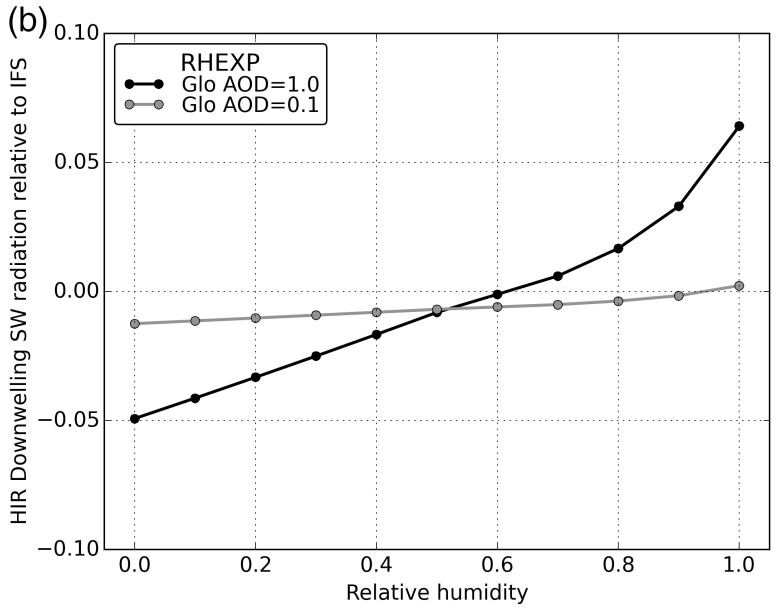

Figure 6. (a) Global, direct and diffuse SWD radiation simulated using the HLRADIA scheme in MUSC for 550 nm AODs of 0.1 and 1.0 and relative humidities varying between 0.0 and 1.0 **(b)** similar to **(a)** but shows the HLRADIA global SWD radiation relative to the IFS scheme which uses a constant relative humidity of 0.8.

ACPD
15, 32519–32560, 2015

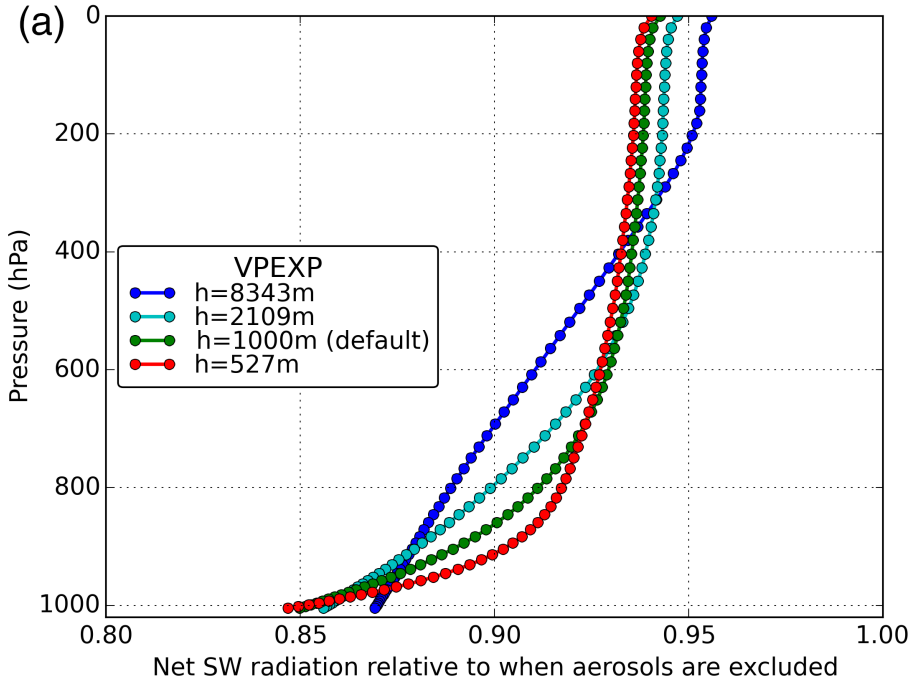

Figure 7.

ACPD
15, 32519–32560, 2015

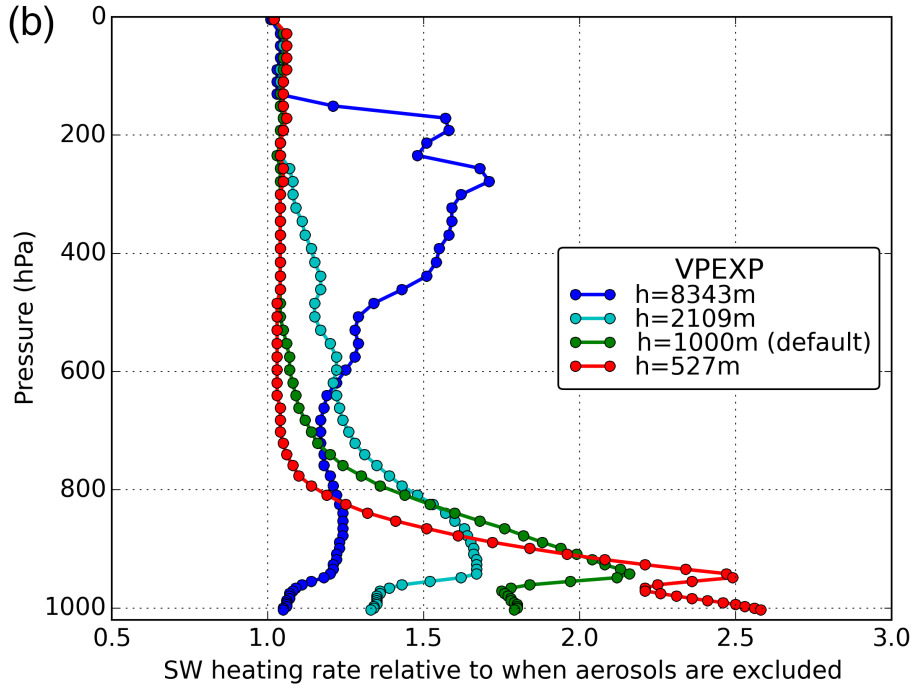

Figure 7. The influence of the vertical scale height (*h*) of land aerosols on **(a)** net SW radiation and **(b)** the SW heating rate as a function of atmospheric pressure relative to the case where aerosols are not included.

ACPD
15, 32519–32560, 2015

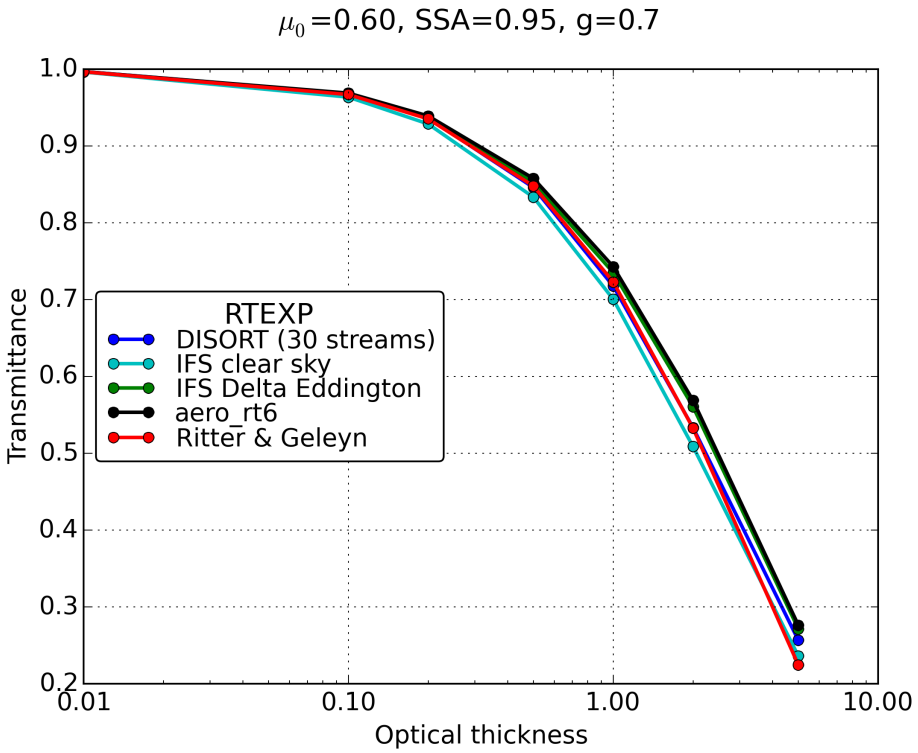

Figure 8. Comparison of layer transmittances calculated using the IFS Delta–Eddington (green curve), IFS clear-sky (blue curve), the HLRADIA (magenta curve) and the ACRANEB2 Ritter and Geleyn (cyan curve) algorithms to the accurate 30-stream DISORT model (red curves). The optical thickness is varied but the cosine of SZA (μ_0) is set to 0.6, g to 0.7 and SSA to 0.95.

ACPD
15, 32519–32560, 2015

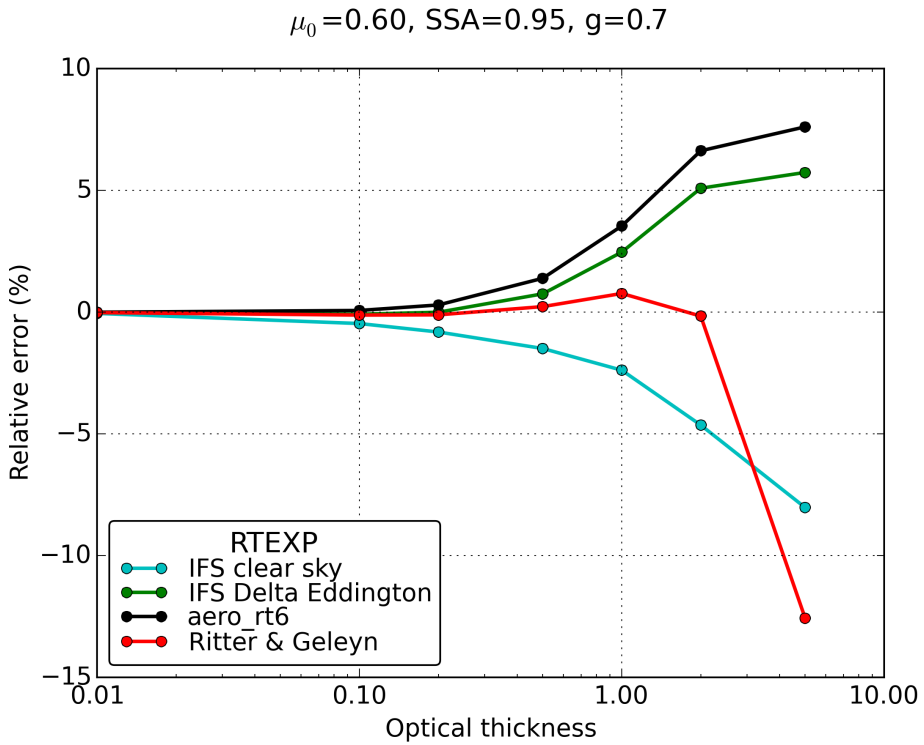

Figure 9. This is similar to Fig. 8 but shows the differences relative to the accurate 30-stream DISORT model.

ACPD
15, 32519–32560, 2015